Photodisintegration of ^{7}Li with progeny nuclei in excited states

W. A. Wurtz
Department of Physics and Engineering Physics, University of Saskatchewan, Saskatoon, Saskatchewan, S7N 5E2, Canada and Canadian Light Source, 44 Innovation Boulevard, Saskatoon, Saskatchewan, S7N 2V3, Canada

R. E. Pywell*
Department of Physics and Engineering Physics, University of Saskatchewan, Saskatoon, Saskatchewan, S7N 5E2, Canada

B. E. Norum and S. Kucuker
Department of Physics, University of Virginia, Charlottesville, Virginia, 22904-4714, USA

B. D. Sawatzky
Temple University/Jefferson Laboratory, Newport News, Virginia, 23606, USA

H. R. Weller and S. Stave†
Triangle Universities Nuclear Laboratory, Duke University, Durham, North Carolina, 27708-0308, USA

M. W. Ahmed
Triangle Universities Nuclear Laboratory, Duke University, Durham, North Carolina, 27708-0308, USA and Department of Physics, North Carolina Central University, Durham, North Carolina 27707, USA

(Received 18 August 2015; published 12 October 2015)

We study the reaction channels $^{7}\mathrm{Li}+\gamma \rightarrow n + {}^{6}\mathrm{Li}(2.19)$, $^{7}\mathrm{Li}+\gamma \rightarrow n + {}^{6}\mathrm{Li}(3.56)$, and $^{7}\mathrm{Li}+\gamma \rightarrow d + {}^{5}\mathrm{He}(1.27) \rightarrow n + d + {}^{4}\mathrm{He}$ by detecting neutrons produced by photodisintegration events. We find absolute cross sections and angular dependence for $^{7}\mathrm{Li}+\gamma \rightarrow n + {}^{6}\mathrm{Li}(2.19)$ at photon energies 13 and 15 MeV and for $^{7}\mathrm{Li}+\gamma \rightarrow n + {}^{6}\mathrm{Li}(3.56)$ at the photon energy 15 MeV. The incident photons are linearly polarized and we report dependence of the cross sections on polarization. For the reaction channel $^{7}\mathrm{Li}+\gamma \rightarrow d + {}^{5}\mathrm{He}(1.27) \rightarrow n + d + {}^{4}\mathrm{He}$ we obtain an upper bound on its cross section at photon energies 12, 13, and 15 MeV.

DOI: 10.1103/PhysRevC.92.044603 PACS number(s): 24.30.Cz, 24.70.+s, 25.10.+s, 25.20.Dc

I. INTRODUCTION

Recent developments of theoretical techniques have allowed accurate calculations of photonuclear reaction cross sections in light nuclei for specific nucleon-nucleon interaction formulations. For example, the Lorentz integral transform method [1] has been applied to the total photodisintegration cross sections of the $A \leqslant 7$ nuclei [2] and to the individual photoneutron and photoproton reaction channels of ^{4}He [3]. Sufficiently precise experimental results can then differentiate between nucleon-nucleon interaction formulations and therefore shed light on the underlying nuclear dynamics.

For the lithium isotopes calculations have been performed for ^{6}Li by Bacca *et al.* [4] but only for the total photoabsorption cross section. Although detailed theoretical calculations for specific reaction channels in light nuclei are possible, lack of experimental data does not provide sufficient incentive for such calculations.

Therefore our group has embarked on a series of measurements on light nuclei using the Duke University High Intensity Gamma Source (HIGS) and the Blowfish Neutron Detector Array to measure all neutron-producing reaction channels for a variety of light nuclei. The first in this series involved measurements on the lithium isotopes.

We have previously reported on the ^{6}Li cross sections [5] and on the $^{7}\mathrm{Li}(\gamma,n_0)\,^{6}\mathrm{Li}$(g.s.) reaction channel [6]. In this work we report an extension of the analysis of our ^{7}Li data to include reaction channels where the progeny nucleus is not in its ground state. Specifically, we wish to obtain cross sections for as many of the reaction channels shown in Table I as possible. These are all the possible reaction channels that include an emitted neutron in the photon energy range of measurements reported in this paper.

In our study of the (γ,n_0) reaction channel we were able to isolate neutrons due to this reaction channel by placing a cut on the light output spectra which eliminated neutrons from all other reaction channels [6]. This was made possible because (γ,n_0) produces neutrons with higher kinetic energies than any other reaction channel. In order to study the rest of the reaction channels, we must employ the methods we developed for studying the photodisintegration of ^{6}Li [5]. In that study, we fit spectra generated from a GEANT4 [7] simulation to our measured spectra.

The analysis reported here is limited to the photon energies 12, 13, and 15 MeV. Data were taken at higher and lower energies; however, data taken at lower energies are either below the thresholds of all reaction channels except (γ,n_0)

*rob.pywell@usask.ca
†Present address: Pacific Northwest National Laboratory, P.O. Box 999, Richland, WA 99352, USA.

TABLE I. Reaction channels to consider in our analysis of the photodisintegration of ^{7}Li at photon energies $\leqslant$15 MeV. The excited state energies are taken from the TUNL nuclear data evaluation [8].

Label	Reaction channel	Threshold (MeV)
(γ,n_0)	$^{7}\mathrm{Li}+\gamma \rightarrow n + {}^{6}\mathrm{Li}$(g.s.)	7.3
(γ,n_1)	$^{7}\mathrm{Li}+\gamma \rightarrow n + {}^{6}\mathrm{Li}(2.19)$	9.5
(γ,d_0)	$^{7}\mathrm{Li}+\gamma \rightarrow d + {}^{5}\mathrm{He}$(g.s.) $\rightarrow n + d + {}^{4}\mathrm{He}$	9.6
(γ,n_2)	$^{7}\mathrm{Li}+\gamma \rightarrow n + {}^{6}\mathrm{Li}(3.56)$	10.9
(γ,d_1)	$^{7}\mathrm{Li}+\gamma \rightarrow d + {}^{5}\mathrm{He}(1.27) \rightarrow n + d + {}^{4}\mathrm{He}$	10.9
(γ,n_3)	$^{7}\mathrm{Li}+\gamma \rightarrow n + {}^{6}\mathrm{Li}(4.31)$	11.6
(γ,p_1)	$^{7}\mathrm{Li}+\gamma \rightarrow p + {}^{6}\mathrm{He}(1.78) \rightarrow p + 2n + {}^{4}\mathrm{He}$	11.8
(γ,n_4)	$^{7}\mathrm{Li}+\gamma \rightarrow n + {}^{6}\mathrm{Li}(5.37)$	12.7
(γ,n_5)	$^{7}\mathrm{Li}+\gamma \rightarrow n + {}^{6}\mathrm{Li}(5.65)$	12.9

or the neutrons produced by the other reaction channels have energies that are too small to be detected. The data taken at higher energies do not allow us to separate reaction channels by fitting to spectra. This is because there are too many reaction channels and they have overlapping neutron kinetic energy distributions. We are able to extract absolute cross sections and associated Legendre polynomial coefficients for the (γ,n_1) reaction channel at 13 and 15 MeV and for (γ,n_2) at 15 MeV. We are only able to obtain an upper bound on the (γ,d_1) cross section at 12, 13, and 15 MeV.

II. EXPERIMENT AND ANALYSIS

The data used in this analysis is the same as was used in our study of the (γ,n_0) reaction channel. As we have described the experimental setup in detail elsewhere, [5,6,9] we will present here only a rudimentary discussion.

The measurements were performed at the High Intensity Gamma-Ray Source (HIGS) [10] at Duke University in Durham, NC, USA. HIGS is able to produce a nearly monochromatic, polarized photon beam through the process of Compton backscattering. These photons were used to initiate photodisintegration events on our natural lithium target.

We detected the produced neutrons using the Blowfish Neutron Detector Array, also known simply as Blowfish [11]. Blowfish is a segmented fast-neutron detector using 88 neutron detecting cells filled with BC-505 liquid scintillator. The cells are arranged in a sphere with the front face of each cell at a radius of 40.6 cm from the center. Blowfish has an angular acceptance of approximately $\frac{1}{4}$ of 4π sr. Using Blowfish we obtain light-output, time-of-flight, and pulse-shape discrimination (PSD) spectra for each detector cell.

As well as measurements with the natural lithium target, we used measurements performed with an enriched ^{6}Li target to subtract the ^{6}Li contribution. An empty target was used to study background neutrons emitted from other sources. We determined that no background subtraction is necessary for the photon energies $\leqslant$15 MeV.

In order to measure the total photon flux, we detect γ rays which Compton scatter from the target into the Blowfish neutron detector cells. Typically we prescale such events in hardware, but we also ran with the prescale function turned off in order to calibrate the use of these events to determine the photon flux times the target thickness, by making use of the known Compton scattering cross section.

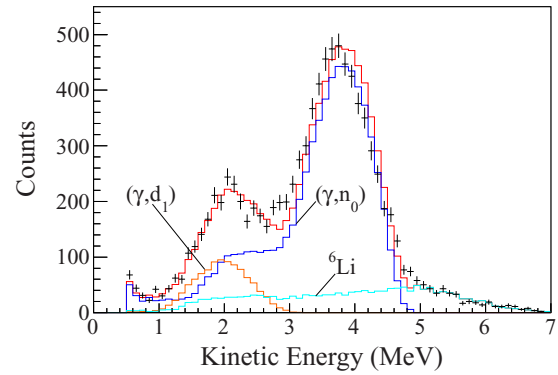

FIG. 1. (Color online) A measured neutron kinetic energy spectra for a particular Blowfish cell at a beam energy of 12 MeV (data points, black). Also shown are the simulations of the (γ,n_0) (blue online) and (γ,d_1) (orange online) reaction channels, and the ^{6}Li contribution (teal online). The histogram through the data points (red online) is the sum of the simulation and ^{6}Li contribution histograms.

To determine the relative neutron yields for each reaction channel, we fit the simulated time-of-flight spectra to the measured time-of-flight spectra. This fitting procedure, and the GEANT4 simulation, were described in detail in our earlier paper on ^{6}Li, so only a brief description is given here. The simulation is run for each reaction channel to produce the expected time-of-flight spectrum for each Blowfish cell. The fit to the measured time-of-flight spectra for each cell is performed by varying only the amplitude of the contribution from each reaction channel, and not the neutron energy or the decay widths, which are obtained from Ref. [8].

From the time-of-flight spectra we can compute neutron kinetic energy spectra and these are shown in Figs. 1, 2, and

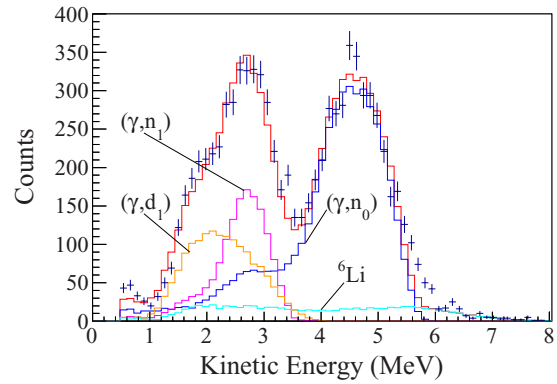

FIG. 2. (Color online) A measured neutron kinetic energy spectra for a particular Blowfish cell at a beam energy of 13 MeV (data points, black). Also shown are the simulations of the (γ,n_0) (blue online), (γ,n_1) (magenta online), and (γ,d_1) (orange online) reaction channels and the ^{6}Li contribution (teal online). The histogram through the data points (red online) is the sum of the simulation and ^{6}Li contribution histograms.

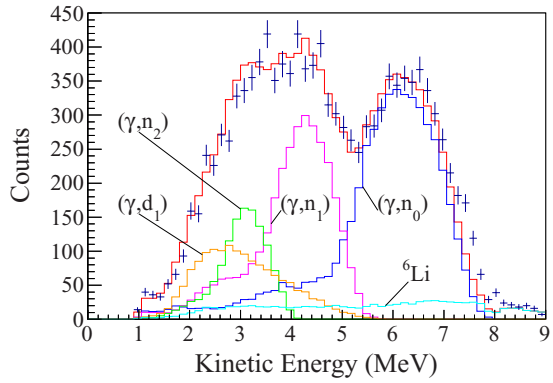

FIG. 3. (Color online) A measured neutron kinetic energy spectra for a particular Blowfish cell at a beam energy of 15 MeV (data points, black). Also shown are the simulations of the (γ,n_0) (blue online), (γ,n_1) (magenta online), (γ,n_2) (green online), and (γ,d_1) (orange online) reaction channels and the ^{6}Li contribution (teal online). The histogram through the data points (red online) is the sum of the simulation and ^{6}Li contribution histograms.

3 for both the measured and the fitted simulated spectra. The low-energy drop-offs in these spectra are due to the neutron detector efficiency going to zero for low-energy neutrons. Note that we do not perform a fit for the (γ,n_0) reaction channel but rather use the previously reported values [6] which were obtained without having to perform a fit to determine neutron yields. For the (γ,n_1), (γ,n_2), and (γ,d_1) reaction channels we determine the neutron yields by fitting spectra.

As discussed in detail in our reporting of the ^{6}Li photoneutron cross sections [5], a limitation of this method is that when two different reaction channels have similar neutron kinetic energy spectra, it is not possible to separate these reaction channels in the fitting procedure. In this analysis the neutron yields for (γ,n_1) and (γ,n_2) are believed to not contain neutrons from any other reaction channel. However, the neutron yields obtained for (γ,d_1) may contain contributions from other reaction channels, such as (γ,d_0), (γ,p_1), (γ,n_3), (γ,n_4), and (γ,n_5). Therefore it is not possible to separate these reaction channels. Instead, we extract a phenomenological set of angular distribution parameters that we can use to simulate the contribution from these overlapping reaction channels in the fit. In the figures the fit for these combined reaction channels are simply labeled (γ,d_1). We then used these phenomenological parameters in the integration to find the total cross section. Therefore, that integration only gives an upper bound on the actual (γ,d_1) cross section.

III. RESULTS

Once we have obtained the neutron yields for (γ,n_1) and (γ,n_2) for each Blowfish cell, we can obtain associated Legendre polynomial coefficients for those reaction channels. We use the associated Legendre function

TABLE II. Measured associated Legendre function coefficient values for the ^{7}Li reaction channels (γ,n_1) and (γ,n_2) at photon energies of 13 and 15 MeV.

Energy	Coefficient	(γ,n_1)	(γ,n_2)
13 MeV	a_1	0.38 ± 0.05	n/a
	a_2	-0.08 ± 0.07	n/a
	e_2	-0.20 ± 0.02	n/a
	e_3	-0.007 ± 0.010	n/a
15 MeV	a_1	0.11 ± 0.01	0.10 ± 0.04
	a_2	-0.14 ± 0.02	-0.68 ± 0.06
	e_2	-0.004 ± 0.006	0.05 ± 0.02
	e_3	-0.010 ± 0.003	0.009 ± 0.009

expansion

$$\frac{d\sigma}{d\Omega}(\theta,\phi) = \frac{\sigma}{4\pi}\left[1+\sum_{k=1}^{\infty} a_k P_k^0(\cos\theta) + \sum_{k=2}^{\infty} e_k P_k^2(\cos\theta)\cos 2\phi\right],$$

where P_k^q are the associate Legendre functions and the a_k and e_k are their coefficients. The angle θ is the polar angle and ϕ is the angle from the polarization vector. The quantity σ is the total cross section while $d\sigma/d\Omega$ is the differential cross section.

We use the GEANT4 simulation to take into account neutron scattering and the finite geometry our our detector system. The simulation is run for each component of the Legendre polynomial expansion to obtain simulated yields for each cell, which are then fitted to the measured yields to obtain the Legendre polynomial coefficients. This procedure, along with the methods used to obtain the reported uncertainties, is detailed more fully in Refs. [9] and [5]. The derived coefficients are reported in Table II.

As was the case with our ^{6}Li analysis [5] we obtain the coefficients a_1, a_2, e_2, and e_3. We are unable to obtain a coefficient a_3 because this coefficient is very susceptible to noise introduced by the fitting procedure. The coefficient e_3 is not as susceptible. Since the (γ,d_1) neutron yields are contaminated with other reaction channels, any angular dependence has no physical meaning. Rather, we obtain a phenomenological a_1 coefficient which we use to reproduce the measured spectra. The phenomenological a_1 values for the (γ,d_1) reaction channel are -0.11 ± 0.14 at 12 MeV, 0.11 ± 0.16 at 13 MeV, and 0.95 ± 0.14 at 15 MeV, with only the last one being distinguishable from zero.

Once the angular dependence of the reaction channels has been determined, we can find the absolute cross section by integrating the angular distribution and using the γ-ray yields and Compton scattering cross sections. The absolute cross sections are reported in Table III.

In the Legendre coefficient fit, we have made no assumptions about which transition matrix elements (TME) contribute to the cross section. Under the assumption that the cross section consists mainly of p-wave $E1$ absorption along with contributions from s-wave $M1$ and d-wave $E2$,

TABLE III. Absolute cross sections for the ^{7}Li reaction channels (γ,n_1) and (γ,n_2), and upper bounds on the absolute cross section of (γ,d_1), at photon energies of 12, 13, and 15 MeV.

Energy (MeV)	(γ,d_1) (mb)	(γ,n_1) (mb)	(γ,n_2) (mb)
12	$\leqslant 0.20 \pm 0.01$	n/a	n/a
13	$\leqslant 0.28 \pm 0.01$	0.080 ± 0.003	n/a
15	$\leqslant 0.25 \pm 0.01$	0.323 ± 0.009	0.124 ± 0.004

and the TME amplitudes are the same for different p-wave and d-wave amplitudes, Weller *et al.* [12,13] have derived relationships between the Legendre coefficients. If the p-wave $E1$ absorption is dominant over the d-wave $E2$ component we would expect that $a_2 \approx -2e_2$. This condition appears to be not satisfied for either reaction channel at either 13 or 15 MeV. This is in contrast to the (γ,n_0) reaction channel [6] where coefficients consistent with $E1$ absorption were observed at these energies. The nonzero e_3 coefficient for the (γ,n_1) channel at 15 MeV is consistent with some $E2$ absorption. Unfortunately further interpretation is not possible since additional coefficients could not be extracted from the data.

IV. CONCLUSION

We have measured the cross section and angular dependence of the reaction channel ^{7}Li(γ,n_1) at photon energies of 13 and 15 MeV and the reaction channel ^{7}Li(γ,n_2) at 15 MeV. The ^{7}Li(γ,d_1) reaction channel could not be completely separated from other reaction channels and therefore we have only been able to estimate an upper bound on the absolute cross section at 12, 13, and 15 MeV, and a meaningful angular dependence could not be determined. We hope that these cross sections along with our previously reported ^{7}Li(γ,n_0) cross section will provide a base for further theoretical study of ^{7}Li photodisintegration.

ACKNOWLEDGMENTS

We acknowledge the financial support of the Natural Sciences and Engineering Research Council of Canada. This research has been enabled by the use of computing resources provided by WestGrid and Compute/Calcul Canada. We thank Johannes Vogt and the staff of the Canadian Light Source for their help in constructing the lithium targets. We would also like to thank the staff of the High Intensity Gamma-Ray Source for their collaboration and the excellent operation of the accelerator. This work comprises part of the thesis of Wurtz [9].

[1] V. D. Efros, W. Leidemann, and G. Orlandini, Phys. Lett. B **338**, 130 (1994).
[2] V. D. Efros, W. Leidemann, G. Orlandini, and N. Barnea, J. Phys. G **34**, R459 (2007).
[3] S. Quaglioni, W. Leidemann, G. Orlandini, N. Barnea, and V. D. Efros, Phys. Rev. C **69**, 044002 (2004).
[4] S. Bacca, N. Barnea, W. Leidemann, and G. Orlandini, Phys. Rev. C **69**, 057001 (2004).
[5] W. A. Wurtz, R. E. Pywell, B. E. Norum, S. Kucuker, B. D. Sawatzky, H. R. Weller, S. Stave, and M. W. Ahmed, Phys. Rev. C **90**, 014613 (2014).
[6] W. A. Wurtz, R. E. Pywell, B. E. Norum, S. Kucuker, B. D. Sawatzky, H. R. Weller, M. W. Ahmed, and S. Stave, Phys. Rev. C **84**, 044601 (2011).
[7] S. Agostinel *et al.*, Nucl. Instr. Meth. A **506**, 250 (2003).
[8] D. R. Tilley, C. M. Cheves, J. L. Godwin, G. M. Hale, H. M. Hofmann, J. H. Kelley, C. G. Sheu, and H. R. Weller, Nucl. Phys. A **708**, 3 (2002).
[9] W. A. Wurtz, Ph.D. diss., University of Saskatchewan, 2010 (unpublished).
[10] V. N. Litvinenko *et al.*, Phys. Rev. Lett. **78**, 4569 (1997).
[11] B. D. Sawatzky, Ph.D. diss., University of Virginia, 2005 (unpublished).
[12] H. R. Weller, J. Langenbrunner, R. M. Chasteler, E. L. Tomusiak, J. Asai, R. G. Seyler, and D. R. Lehman, At. Data Nucl. Data Tables **50**, 29 (1992).
[13] H. R. Weller, R. M. Chasteler, B. S. Marks, R. G. Seyler, and D. R. Lehman, At. Data Nucl. Data Tables **58**, 219 (1994).